Cross-Hemispheric Transport of the Hunga Aerosol Plume: In Situ Evidence and Radiative Effects from the Northern Hemisphere

Corinna Kloss[1], Gwenaël Berthet[2], Pasquale Sellitto[3,4], Irene Bartolome Garcia[5,1], Emmanuel Briaud[2], Rubel Chandra Das[6], Séphane Chevrier[2], Nicolas Dumelié[7], Lilian Joly[7], Thomas Lecas[2], Pauline Marbach[1], Felix Ploeger[1,8], Jean-Baptiste Renard[2], Jean-Paul Vernier[6,7,9], Frank G. Wienhold [10], and Michaela I. Hegglin[1,8,11]

[1]Forschungszentrum Jülich GmbH, Institute of Climate and Energy Systems - Stratosphere (ICE-4), Jülich, Germany
[2]Laboratoire de Physique et Chimie de l'Environnement et de l'Espace, CNRS/Université d'Orléans, UMR 7328, Orléans, France
[3]Univ. Paris-Est Créteil and Université de Paris Cité, CNRS, Laboratoire Interuniversitaire des Systèmes Atmosphériques, Institut Pierre Simon Laplace, Créteil, France
[4]Istituto Nazionale di Geofisica e Vulcanologia, Osservatorio Etneo, Catania, Italy
[5]Institute for Atmospheric Physics, Johannes Gutenberg University Mainz, Mainz, Germany
[6]National Institute of Aerospace, Hampton, USA
[7]GSMA, UMR CNRS 7331, Université de Reims Champagne-Ardenne, Reims, France
[8]Institute for Atmospheric and Environmental Research, University of Wuppertal, Wuppertal, Germany
[9]NASA-Langley Research Center, Hampton (VA), USA
[10]Federal Institute of Technology (ETHZ), Zurich, Switzerland
[11]Department of Meteorology, University of Reading, Reading, UK

Correspondence: Corinna Kloss (c.kloss@fz-juelich.de)

Abstract. The Hunga Tonga–Hunga Ha'apai eruption ($20°$S) in January 2022 injected a substantial amount of water vapor and aerosols into the stratosphere, primarily impacting the Southern Hemisphere and tropics. Using a combination of satellite observations and in situ measurements with optical particle counters, we show that a significant portion of the aerosol plume was transported into the Northern Hemisphere (NH) mid-latitudes. This cross-hemispheric transport occurred within the tropically

5 controlled transition zone, within the shallow branch of the Brewer–Dobson circulation. By October 2022, enhanced aerosol concentrations were observed up to $50°$N, at altitudes between 17 –23 km with some dense plumes at around 21–22 km. In situ observations reveal an effective radius of around 330 nm, comparable to what was observed in the Southern Hemisphere (SH). Aerosol extinction coefficients in the mid-latitudes (30–50$°$N) increased by ∼50% over background levels, corresponding to an aerosol optical depth (AOD) increase of $(1$–$2) \times 10^{-3}$. These enhancements led to a modest, but not negligible,

10 shortwave top-of-atmosphere (TOA) radiative forcing of -0.05 ± 0.01 W m^{-2} between October 2022 and April 2023. Our results show that the moderate aerosol impact of the Hunga eruption in the SH produced non-negligible radiative impacts in the NH, emphasizing the importance of considering both hemispheres when analysing the total impact.

1 Introduction

15 The Hunga volcano (Kingdom of Tonga, 20°S, 175°W) eruptions on January 15, 2022, resulted in the most significant stratospheric aerosol perturbation observed since the eruption of Mt. Pinatubo in 1991 (Sellitto et al., 2022). The eruption injected relatively small amounts of sulfur dioxide (SO_2) (e.g., Carn et al., 2022; Sellitto et al., 2024b) and an unprecedented amount of water vapor into the upper stratosphere (Millán et al., 2022; Khaykin et al., 2022), reaching altitudes of up to 58 km (Taha et al., 2022; Proud et al., 2022; Carr et al., 2022). The SO_2 mass injection was initially estimated at a moderate 0.6–0.7 Tg

20 (Carn et al., 2022) to over 1.0 Tg (Sellitto et al., 2024b), which is at least 15–20 times smaller than that of the Pinatubo eruption (Guo et al., 2004) and no larger than more recent moderate stratospheric eruptions (e.g., Andersson et al., 2015). Nevertheless, the aerosol load, in terms of stratospheric aerosol optical depth (sAOD), was recorded as the largest since Pinatubo (Taha et al., 2022; Sellitto et al., 2022), but peak values are not significantly larger than what was observed following Raikoke (Vernier et al., 2025). The rapid oxidation of SO_2 to sulfate aerosols was accelerated by the elevated levels of water vapor, leading to an

25 unusually fast formation of stratospheric aerosols, with e-folding times between 2 and 4 weeks (e.g., Zhu et al., 2022; Sellitto et al., 2024b; Asher et al., 2023; Legras et al., 2022).

Satellite and in situ observations have provided valuable insights into the evolution and transport of the Hunga aerosol plume. After a transient phase of a few days after the eruption, the plume consisted mainly of water vapour, SO_2, and submicron sulfate particles, with no significant amounts of ash. SO_2 levels returned to background concentrations by the end of January

30 2022 (Shikwambana et al., 2023; Legras et al., 2022; Sellitto et al., 2024b). For the first three months, the sulfate aerosol plume was primarily confined between 20°N and 35°S due to the zonal symmetry of the summer stratospheric circulation (Legras et al., 2022). Marked anomalies in the sAODs were observed at southern hemispheric mid- and high-latitudes starting from April 2022 (Sellitto et al., 2024b). In addition, small filamentary portions of the plume had already reached the northern and southern hemispheric poles by April 2022 (Taha et al., 2022) and were observed above China (at 27°N) with in situ aerosol

35 instruments (POPS and COBALD, Bian et al., 2023). One year later, aerosols from the eruption have been measured in the Antarctica (Deshler et al., 2024). Those in situ observations in Antarctica revealed significant increases in aerosol mass, surface area, and extinction, particularly for particles larger than 0.5 μm (Deshler et al., 2024). During the first 13 months, the descent rate of the aerosol layer was estimated at -0.008 km/day, suggesting that volcanic aerosols could remain in the stratosphere until at least the first half of 2025 (Sicard et al., 2025).

40 Recent analyses of the Hunga aerosol plume have also examined the evolution of the particle size distribution over time. Using data from the Stratospheric Aerosol and Gas Experiment III on the International Space Station (SAGE III/ISS), Duchamp et al. (2023) and Knepp et al. (2024) found that the particle size distribution (effective radius at 400 nm and mode width at 1.25) remained relatively stable over 15 months (March 2022 to June 2023).

Radiative transfer simulations and observational studies have demonstrated the significant impact of the Hunga eruption on

45 the Earth's radiation budget. During the first two weeks, radiative forcing was initially dominated by aerosol-induced cooling, but as the vertical distribution of the plume evolved, water vapor's positive effect began to influence the top-of-the-atmosphere radiative forcing, leading to a net warming effect for the Hunga plume, about 1 month after the eruption (Sellitto et al., 2022).

Over the 13 months following the eruption, after horizontal dispersion and vertical separation of the aerosol and water vapor plumes, the overall radiative forcing of the Hunga plume was found to be negative, with a stratospheric tropical temperature

50   decrease of around 4 K from February to April 2022 and still a very small cooling effect through 2022 and 2023 (Schoeberl et al., 2024, 2022).

While the transport, evolution, radiative impact, and chemical processes of the Hunga plume in the SH have been extensively studied, its impact on the Northern Hemisphere (NH) has not yet been studied in detail and quantified. In this study, we analyze the transport of the Hunga aerosol plumes to the NH and their radiative forcing using a combination of satellite and in situ

55   observations alongside radiative transfer simulations.

2   Methods

2.1   The Lightweight Optical Aerosol Counter, LOAC

LOAC was deployed to measure aerosol properties in the atmosphere (Renard et al., 2016). We use version 1.5, which includes improvements over Renard et al. (2016), featuring increased laser source power and reduced stray light through the design of a

60   new optical chamber. This compact instrument, together with batteries (flight configuration), weighs 1 kg, provides information on the aerosol size distribution from 200 nm to 50 μm (at a wavelength of 650 nm), partial aerosol concentrations, and a coarse classification of aerosol types. The measurement uncertainties depend on the aerosol concentration, flow rate, and sampling frequency, with an estimated 20% uncertainty for concentrations greater than 1 cm^{-3}, increasing to 60% uncertainty for lower concentrations due to Poisson statistical limitations.

65   The time sampling achieved by LOAC is 10 seconds. The temporal resolution of the final profile ranges from 1 to 10 minutes in the upper troposphere and lower stratosphere (UTLS), depending on local particle concentrations and balloon ascent speed, affecting the vertical resolution of the profile. These parameters ensure that LOAC can capture detailed aerosol profiles while accounting for variability in atmospheric conditions.

Aerosol counting observations have been converted to extinction coefficients at 500 nm using a Mie scattering model assuming

70   sulphuric acid droplets. Here, we use LOAC measurement profiles from Reims, France (49.3°N, 4.0°E), obtained on October 19, 2022, from Orleans, France (47.8°N, 1.9°E) on December 06, 2022 and June 02, 2023, and from MeteoModem, France (48.3°, 2.6°E) on November 14, 2022, January 20, 2023 and February 21, 2023.

2.2   Portable Optical Particle Spectrometer, POPS

POPS observations were part of the same payload as the LOAC flight (see above). POPS measures aerosol properties in the

75   atmosphere and weighs around 1 kg, including batteries (Todt et al., 2023). The instrument provides data on aerosol size distributions ranging from 140 nm to around 2.5 μm, measured at a wavelength of 405 nm, as well as partial aerosol concentrations. Measurement uncertainties from Poisson statistics result in uncertainties of approximately 7% for concentrations exceeding 1 cm^{-3}, increasing up to 73% for concentrations below 10^{-2} cm^{-3}. These uncertainties are influenced by predefined instrument

parameters and ambient conditions.

80 The temporal sampling for POPS is 1 second. In the UTLS, POPS can achieve a vertical resolution of ∼50 m. This combination allows for high-resolution temporal and spatial profiling of aerosols in varying atmospheric conditions. POPS size distributions have also been converted to extinction at 500 nm. For the measurement flights considered in this study, data obtained above approximately 25 km altitude were excluded due to a collapse of the volumetric flow rate at those altitudes.

In this study, we use POPS profiles measured from Reims, France (49.3°N, 4.0°E), obtained on October 12, 2022, and October 85 19, 2022, and from Orleans, France (47.8°N, 1.9°E), on December 06, 2022.

2.3 Ozone Mapping Profiler Suite Limb Profiler, OMPS-LP

OMPS-LP, onboard the Suomi National Polar-orbiting Partnership (Suomi NPP) satellite, measures limb-scattered radiance and solar irradiance across the 290–1000 nm wavelength range, covering altitudes from 0 to 80 km with a vertical sampling of 1 km and an instantaneous resolution of 1.5 km (Jaross et al., 2014). The instrument provides near-global coverage within 90 3–4 days using three horizontally separated vertical slits. Aerosol extinction coefficient profiles are derived from radiance measurements at 675 nm.

With its high sampling rate, meaning near-global coverage every few days, we use OMPS observations here to study transport features of the respective volcanic plume. This study utilizes version 2.0 aerosol extinction data (Taha et al., 2021) for the years 2022 and 2023, mainly focusing on the northern hemispheric stratosphere.

95 2.4 Stratospheric Aerosol and Gas Experiment III, SAGE III/ISS

SAGE III/ISS, launched in February 2017 and operational on the International Space Station (ISS) since June 2017, measures profiles of trace gases and aerosol extinction coefficients using solar and lunar occultation, as well as limb scatter. The instrument operates across nine wavelengths ranging from 384 to 1544 nm, acquiring approximately 30 profiles daily within latitude bands of 60°N–60°S, with optimal spatial coverage in mid-latitudes (30°–60°N/S).

100 Aerosol extinction coefficient profiles extend vertically from ∼40 km down to the Earth's surface, or to the limit of the detector's dynamic range, which is typically constrained by optically thick water clouds. The vertical resolution is ∼1 km, with data reported at 0.5 km intervals between 0.5 and 40 km. The instrument has a horizontal resolution of ∼200 km along the line of sight and an additional 200 km along the ISS's motion. Tropopause height and meteorological parameters are obtained from the Modern-Era Retrospective analysis for Research and Applications version 2 (MERRA-2) reanalysis data to support aerosol 105 extinction retrievals.

This study utilizes version 5.30 of the cloud-unfiltered solar occultation aerosol extinction coefficient profiles at multiple wavelengths (384, 449, 521, 602, 676, 756, and 869 nm). These data are primarily used to calculate the radiative impact of the northern hemispheric aerosol enhancement following the Hunga eruption. Additionally, SAGE III/ISS observations at 756 nm are employed to validate aerosol plume signatures detected by optical particle counters (OPCs), ensuring consistency across 110 measurement techniques.

2.5 CALIPSO Backscatter Initialized LaTM Trajectory Analysis

To study the transport of the Hunga plume, the Langley Trajectory Model (LaTM) (Fairlie et al., 2014) is initialized using backscatter data from the CALIOP/CALIPSO satellite in conjunction with MERRA-2 meteorological data. We used CALIPSO level 1 V4-51 to initialize the LaTM after averaging the data over approximately 1degree latitude along the orbit track and

115 removing clouds using a depolarization threshold of 5% (Vernier et al., 2009). The analysis focuses on the air parcels that traveled over France, as illustrated in Fig. A3.

2.6 Chemical Lagrangian Model of the Stratosphere

To compute backward trajectories we used the trajectory module of CLaMS (Chemical Lagrangian Model of the Stratosphere, (McKenna et al., 2002a, b; Pommrich et al., 2014) and references therein). CLaMS is a modular chemistry transport model

120 developed to study transport and chemistry processes in the atmosphere. The backward trajectories were run during seven days and driven by ERA5 reanalysis data truncated to $1° \times 1°$. latitude/longitude resolution and sampled every 6 hours (00, 06, 12, 18 UTC). For more details about the used ERA5 version, the reader is referred to Ploeger et al. (2021) and (Hersbach et al., 2020). The calculation of the 9 trajectories was initiated on the 19/10/2022 in a box targeting the area of the in situ observations (48°N–51°N, 3.5°E–6.5°E, 20–20.6 km). In total, 63 backward trajectories were calculated with output (on i.e.

125 potential temperature, pressure, longitude and latitude) every 15 minutes.

2.7 UVSPEC Radiative Transfer Model

The UVSPEC radiative transfer model, part of the LibRadtran package (Mayer and Kylling, 2005), is used to estimate shortwave radiative forcing of the stratospheric aerosol perturbation in the Northern Hemisphere due to the Hunga plume transport. The UVSPEC solves the radiative transfer equation using the SDISORT method, which employs the pseudo-spherical approxi-

130 mation of the discrete ordinate method (DISORT) (Dahlback and Stamnes, 1991). The molecular absorption was parameterized with the LOWTRAN band model (Pierluissi and Peng, 1985), as adopted from the SBDART code (Ricchiazzi et al., 1998). With UVSPEC, we computed the top-of-atmosphere (TOA) direct and diffuse shortwave spectra in the spectral range covered by the SAGE III/ISS observations (385–1550 nm), with a spectral resolution of 0.1 nm. Input solar flux spectra are taken from (Kurucz, 2005), and atmospheric conditions are based on the AFGL climatological standard winter midlatitude atmo-

135 sphere (Anderson et al., 1986). We estimated the northern-hemispheric perturbation of the Hunga eruption by comparing the Hunga-perturbed period with a background period for the stratospheric aerosol. For more details, see Sect. 3.5.

3 Results and Discussions

3.1 Stratospheric aerosol overview in the Northern Mid-Latitudes 2021–2024

The general stratospheric aerosol situation in the northern mid-latitudes, for the period 2021–2024, is visualized in Fig. 1.

140 Throughout the whole time, no background aerosol conditions are observed. Following the La Soufrière eruption in April 2021
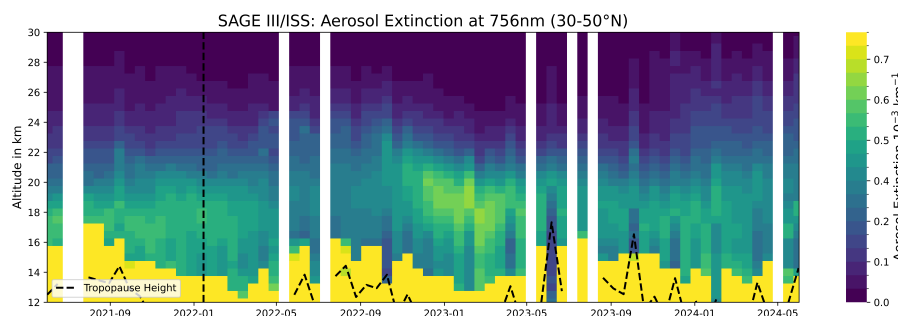
Figure 1. SAGE III/ISS aerosol extinction observations at 756 nm for the northern mid-latitudes (30–50°N). Vertical dashed lines represent the timing of the main eruptions at Tonga. No cloud filter is applied. The horizontal dashed line shows the average MERRA-2 tropopause height for the respectively averaged SAGE III/ISS extinction profiles. The vertical dashed line represents the timing of the Hunga eruption.

at 13°N and 61°W, the stratospheric northern mid-latitudes were significantly affected by an increased aerosol load (e.g., Li et al., 2023; Bruckert et al., 2023; Taylor et al., 2023). From Fig. 1, the increase is evident up to around 22 km altitude until early 2022. The exact phase-out time of aerosols from La Soufrière cannot clearly be identified, because the Hunga eruption (at 20°S, 175°W) in January 2022 produced a slight influence on the northern-hemispheric stratosphere as early as March 2022

145 (Taha et al., 2022).

Therefore, because of already enhanced background conditions in the stratospheric northern mid-latitudes, the actual beginning of the general influence of the Hunga eruption on the NH in terms of increased aerosol values cannot clearly be identified. However, a significant increase in aerosol extinction from October 2022 to May 2023 between 16 and 23 km (around 4 km above the respective tropopause) altitude, with peak enhancements around December 2022/January 2023, can clearly be

150 associated with enhancements from the Hunga eruption.

Even though the eruption at La Soufrière occurred in the NH with direct stratospheric injections of sulfur-containing gaseous and aerosol species, its impact, as seen in Fig. 1, in terms of aerosol extinction is by a factor of around 1.5 smaller than that of the Hunga eruption.

3.2 In Situ Observations of the Hunga Plume in the Northern Mid-Latitudes

155 In situ observations with Optical Particle Counters (LOAC and POPS) confirm an enhanced aerosol layer in the northern-hemispheric mid-latitudes, which can be associated with the transport of the Hunga plume. We highlight two in situ measurement profiles from a weather balloon flight in Reims, France, on October 19, 2022, which are analyzed in more detail throughout this manuscript and reveal a peak aerosol plume layer between 20 and 23 km altitude (see Fig. 2a and b, black profiles and Figure A1a and b, respectively). While Fig. 1 shows that the overall aerosol impact in the NH extends to lower

160 altitudes down to 16 km, the POPS and LOAC measurement profiles from 19/10 indicate the influence of a concentrated, dense plume patch at 20–23 km altitude. Reference measurement flights on October 12, 2022, December 6, 2022 and June 2, 2023 in France (Fig. 2a and b), do not show such a clear increase of a localized transport feature in aerosol extinction at those altitudes
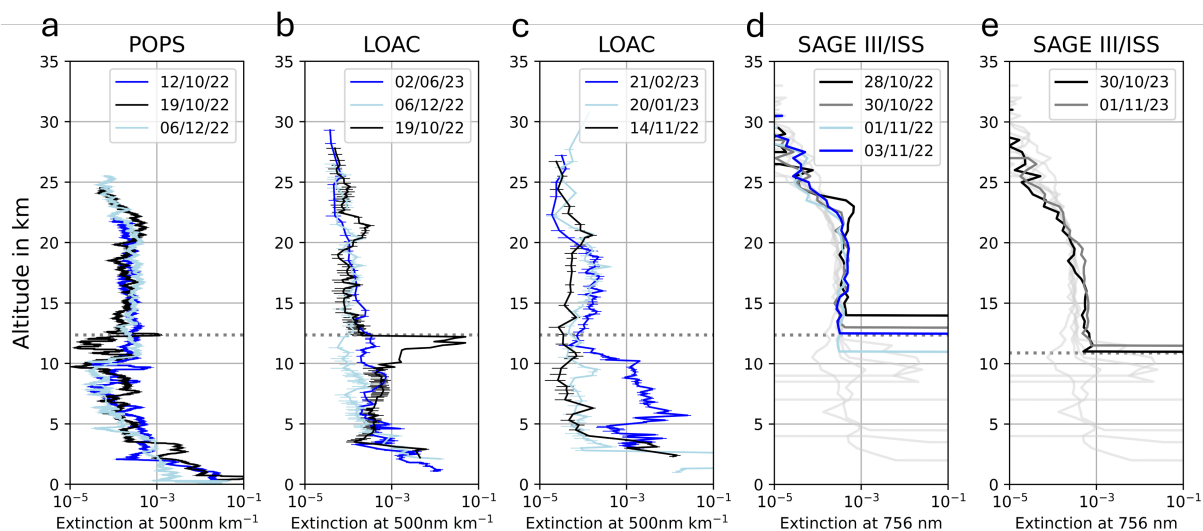
Figure 2. (a) POPS in situ aerosol partial extinction observations for the plume signal from Reims, France 19/10/2022 at 49°N and 4°E and comparison flights for background measurements on 06/12/2022 (Orleans, France, 47.8°N, 1.9°E) and 12/10/2022 (Reims); (b) Respective LOAC v1.5 observations, including background measurements on 02/06/2023 (Orleans, France, 47.8°N, 1.9°E); (c) LOAC observations of aerosol plumes of volcanic origin from MeteoModem, France 48.3°N, 2.6°E; (d) Closest SAGE III/ISS (at 756 nm) aerosol extinction profiles compared to the POPS in (a) and LOAC (b) measurements on 19/10/2022, at 47.08°N, 3.23°E at 06:28 UTC on 28/10/2022 in black; 4.39°E, 48.27°N at 6:30 UTC on 30/10/2022 in grey; 4.85°N, 48.1°E at 6:30 UTC on 1/11/2022 in light blue; 4.46°N, 46.54°E at 6:31 UTC on 3/11/2022 in blue. Horizontal dotted grey lines represent the tropopause height by MERRA-2 on 19/10/2022. (e) Comparable SAGE III/ISS observations in space and time of the year, but one year later for background conditions at 48.6°N, 0°E, 30/10/2023 in black and 47.6°N, 0.1°E, 01/11/2023 in grey. Light grey lines in (d) and (e) represent background profiles observed in 10/2018 above central Europe.

(20–23 km). This is further confirmed by other OPC and in situ observations as shown in the supplementary material Fig. A1 and A2. The SAGE III/ISS aerosol extinction measurements, taken closest in time and space to the in situ measurement flight
165 shown in Fig. 2a and b, confirm the observed enhancement above 20 km altitude (Fig. 2d, black profile). A smaller but still increased aerosol signal above 20 km is observed in France on 14/11, one month after POPS and LOAC measurements have identified a dense plume (black profile, Fig. 2c). Other observations by LOAC in France in 2022 and 2023 in Fig. 2c show aerosol enhancements between 15 and 20 km altitude, consistent with what is seen in Fig. 1.

The general aerosol enhancement above the tropopause up to 20 km altitude is clear when comparing SAGE III/ISS observa-
170 tions in fall 2022 with those in 10/2018 under mostly unperturbed stratospheric conditions and still visible one year later in 2023 (Fig. 2d and e).

To trace back in space and time the aerosol plumes observed in the POPS and LOAC measurements discussed above, we performed back-trajectory calculations (initialized from a 2° by 2° grid around Reims, France at 20.6 km altitude) using the Chemical Lagrangian Model of the Stratosphere (CLaMS) and analyzed satellite-based aerosol extinction observations
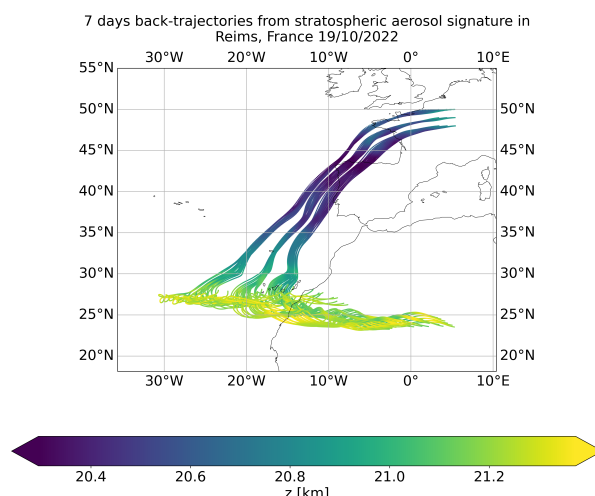
Figure 3. Simulation depicting the backward trajectories of 9 air parcels over 7 days with hourly outputs using CLaMS. The air parcels originate from a region defined as a box spanning 48°–50°N and 3°–5°E at 20.6 km altitude. Colors represent the corresponding altitude levels.

175 from OMPS; this is shown in Fig. 3 and 4. The back trajectories indicate a clear transport pathway along isentropes from the tropics/mid-latitudes (on October 12, 2022, around 25°N and between 0° and 30°W at approximately 21.2 km altitude) to the location of the POPS and LOAC in situ observations in Reims (on October 19, 2022, at 49°N and 4°E at around 20.6 km altitude). Fig. 4 presents spaceborne aerosol extinction observations from OMPS, illustrating how a portion of the aerosol plume originating from the tropical stratosphere due to the Hunga eruption detached and formed a compact plume

180 transported toward the northern mid-latitudes. Because the longitude ranges in Fig.4a–d were selected based on the CLaMS back trajectories shown in Fig.3, the OMPS aerosol extinction plume transport observations clearly confirm the pathways indicated by the trajectories.

A distinct increase in aerosol extinction is observed at around 12 km altitude, below the tropopause on October 19, 2022 (Fig. 2b). This increase is clearly detected by LOAC but is much less pronounced in POPS observations. At this altitude,

185 LOAC identifies a particle population with sizes extending up to its upper measurement limit of 50 μm, with some particles identified as ice (cirrus clouds). Since POPS has an upper size detection limit of ~3 μm, larger particles are not detected, explaining the observed differences in partial extinction between the two instruments.

Figure 5 presents a complementary method for verifying the source of the observed enhanced aerosol values above France, as shown in Fig. 2. This analysis employs the CALIPSO Backscatter Initialized LaTM Trajectory Analysis data to provide

190 higher vertical resolution backscatter information regarding the transport of the aerosol plume from the Hunga eruption. The time series analysis of backscatter ratios over France was derived from the trajectory analysis using this methodology. The data reveal a distinct signature of elevated backscatter (ratios greater than 1.1) in regions at altitudes of approximately 20 to 22 km in mid-October 2022. This coincides with the timeline of balloon measurements recorded on October 19, 2022, at 6:30 UTC
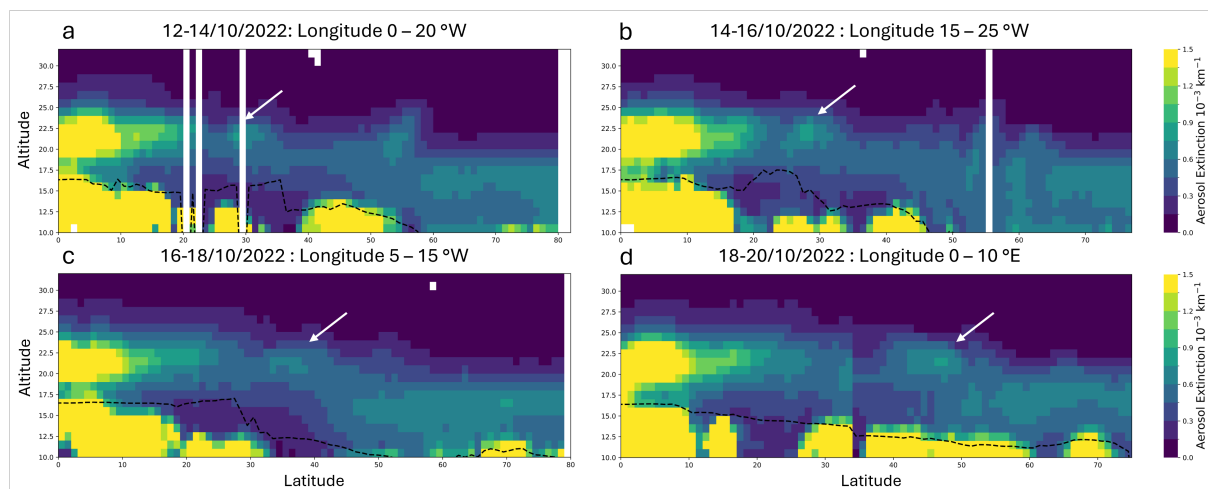
Figure 4. OMPS aerosol extinction observations at 675 nm. The dashed black line represents the tropopause altitude according to MERRA-2.
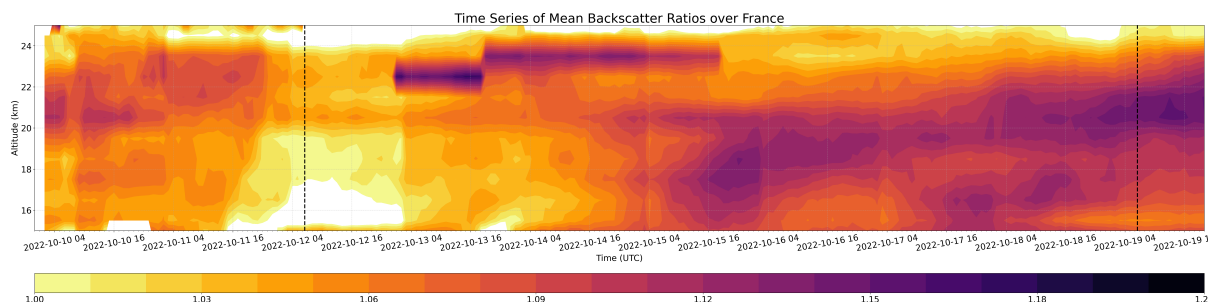
Figure 5. Time series of mean backscatter ratios over France as observed by CALIOP/CALIPSO. The mean profile is calculated within a 1 km altitude bin, using data from a 1000 km radius around Reims (49.26°N, 4.03°E). The black dashed lines indicate the timing of the balloon measurements.

(as seen in Fig. 2). These observations with respective analysis give an independent confirmation, with an alternative data set, that the Hunga plume has reached the NH mid-latitudes during that time.

3.3 Transport and Distribution in the Northern Hemisphere

The horizontal distribution of the Hunga aerosol plume toward the NH is visualized in Fig. 6 and in the supplementary video, which show stratospheric aerosol extinction observations from OMPS across 0°–90°N at 21–22 km altitude. While it has to be noted that the impact on the stratospheric NH ranges from 17 to 23 km altitudes as seen in Fig. 1, distinct filaments closer to altitudes at around 20 km have been found. Therefore, Fig. 6 focuses on the representation of denser aerosol plumes/filaments transported to the NH mid-latitudes. These features appear primarily in the altitude range around 21–22 km and latitudes poleward of the tropics.

From late January to February 2022, the tropical stratosphere (at 21–22 km altitude) up to 10°N becomes increasingly filled with aerosol particles originating from the Hunga eruption. From that point until late March 2022, observations reveal trans-
205 port of distinct but rather light aerosol plumes (in terms of aerosol extinction enhancements) are observed being transported to higher latitudes in the NH to around 35°N.

By the end of March 2022, most of the tropical to subtropical regions up to 20°N are filled with aerosols. Distinct filaments continue to move northward, reaching approximately 40°N. From October 2022 until January 2023, denser and more extensive plumes (in both latitude and longitude) are transported to higher latitudes, with the filaments slowly getting mixed with the
210 surrounding background air.

The distributions in Fig. 6 further reveal that northward transport of the aerosol plume is related to streamers extending from the subtropics to middle latitudes which are likely caused by Rossby wave breaking. At levels around 500K (20-21km), such poleward transport related to breaking Rossby waves has been shown to maximize during boreal winter (Homeyer and Bowman, 2013), consistent with increased northward transport of Hunga aerosol from end of October onwards.

215 The most significant impact of the Hunga aerosol plume to the NH mid-latitudes is therefore observed in the NH winter (Fig. 6 and Fig. 1). This increase during winter months is also confirmed with additional in situ observations as presented in the supplementary material (Fig. A2). The impact of the Hunga aerosols to the NH mid-latitude stratosphere remains evident until around April 2023. Dense signals such as those observed in February 2023, at around 60°N, show rather the influence of polar stratospheric clouds and are therefore not related to the Hunga aerosol signature. The aerosol enhancements observed with
220 POPS and LOAC (Fig. 2a and 2b) are consistent with filament observations shown in the supplementary video, particularly in mid-October at around 50°N and 150°E. The tropical stratosphere shows an enhanced aerosol signal until September 2023, while aerosol filaments transported to the northern mid-latitudes decrease in intensity. By the end of 2023, the aerosol signal in the tropical stratosphere decreases and with that the extent of the transported filaments towards the north.

These transport patterns are consistent with those found in earlier studies revealing a direct transport pathway between the
225 tropics and midlatitudes within the first few kilometers above the tropical tropopause (around 100–50 hPa or 16–21 km), before the air enters the tropical pipe within which mixing with midlatitude air is inhibited through very strong potential vorticity gradients (Plumb, 2002). Our results thereby strongly resemble the transport feature seen in Fig. 1 of Grant et al. (1994), in which aerosol observations following the 1991 Pinatubo eruption clearly reveal poleward transport out of the tropical region in this altitude range.

230 This region roughly corresponds to the tropically controlled transition layer, a term coined by Rosenlof et al. (1997), within which air, after passing through the tropical cold point tropopause and being dehydrated, is mixed horizontally into the midlatitudes. Hegglin and Shepherd (2007) further revealed a strong seasonality in the strength and depth of the mixing within this layer based on O_3–N_2O correlations. Ultimately, the meridional mixing stems from the breaking of synoptic-scale Rossby waves above the subtropical jet (Trepte and Hitchman, 1992; Haynes and Shuckburgh, 2000; Shepherd, 2000).
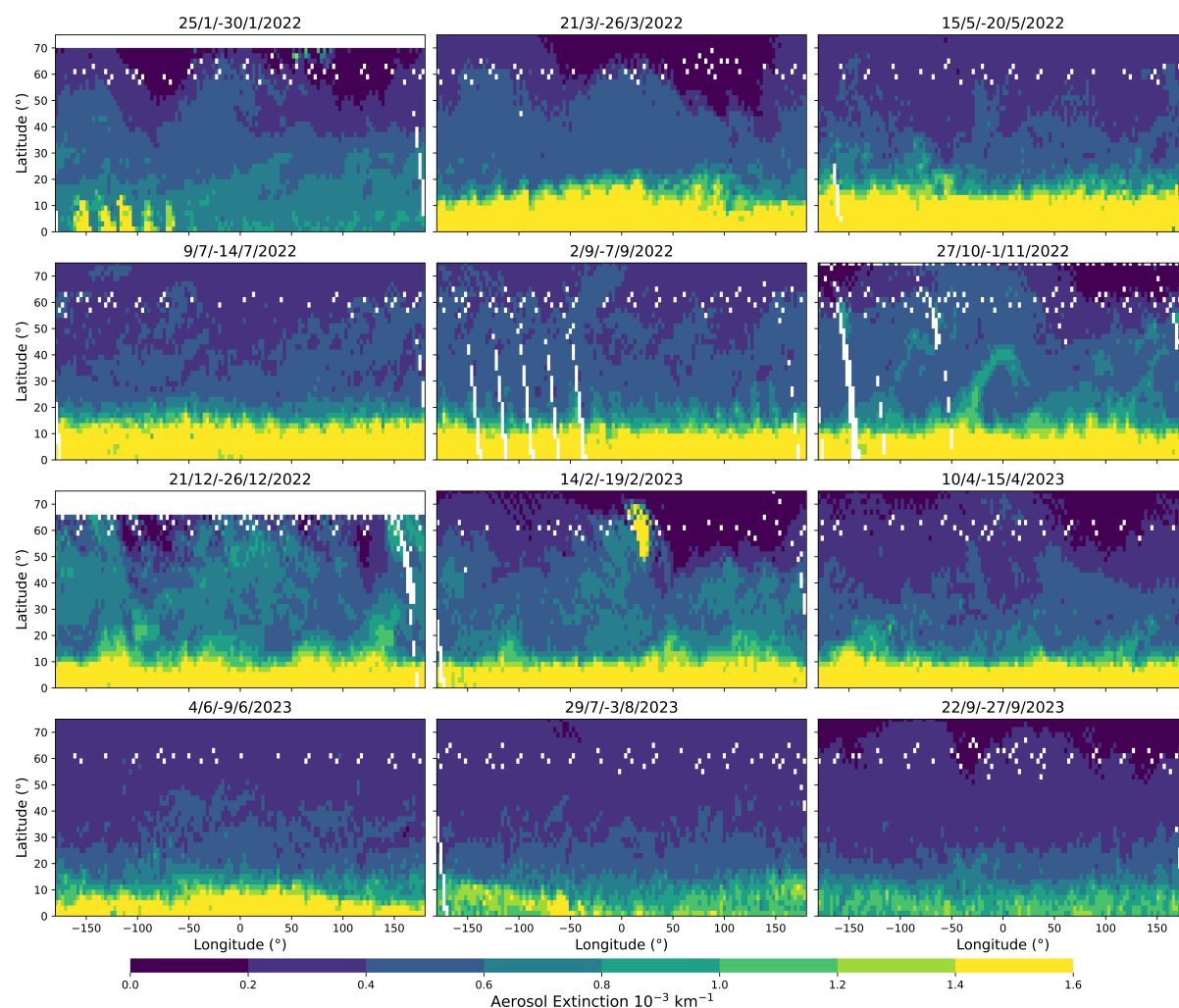
Figure 6. OMPS aerosol extinction observations at 675 nm, horizontal view at 21–22 km altitude in the NH from January 2022 to January 2024. The respective detailed transport is shown in the Supplementary material video.

3.4 Aerosol Size Distribution and Microphysical Properties

Figure 7 presents the aerosol size distribution within the aerosol plume layer (20–22.5 km), based on profiles from Fig. 2a (POPS) and Fig. 2b (LOAC), observed in Reims, France, on 19 October 2023. No significant variation is observed between the lower and upper plume layers (i.e. 20–21 km and 21.5–22.5 km), suggesting a homogeneous size distribution across this altitude range—i.e., no notable sedimentation within the layer.

Statistical tests confirm that the POPS data are significantly better fit by a bimodal than a unimodal distribution. A bimodal lognormal distribution was fitted to the POPS data using the method described by Brock et al. (2021) and Deng et al. (2022).

Table 1. Fitted parameters for the bimodal lognormal distribution derived from POPS measurements, as shown in Fig. 7. The table lists the peak concentration, mode radius, effective radius, and geometric standard deviation (σ) for each mode.

Parameter	Mode 1	Mode 2
Peak Concentration	$8.43\,\mathrm{cm}^{-3}/\mu\mathrm{m}$	$0.64\,\mathrm{cm}^{-3}/\mu\mathrm{m}$
Mode Radius	97.12 nm	327 nm
Effective Radius	151 nm	425 nm
σ	1.4	1.3
Total Effective Radius = 327 nm		

The combined lognormal fits yield the total bimodal distribution. Parameters derived from the fit are listed in Table 1.

For OPC measurements six months later, Deshler et al. (2024) also report a bimodal pattern in the Southern Hemisphere (Antarctica), even though the observed particle size of the second mode in Deshler et al. (2024) is larger ($\sim$900 nm compared to 330 nm with POPS) .

The overall effective radius derived from POPS is 327 nm (weighted from the two modes, Table 1). This agrees well with in situ measurements over Antarctica (200–300 nm, Deshler et al. 2024) and is lower than remote sensing retrievals from January–June 2023, which suggest values between 400–500 nm (Duchamp et al., 2023; Boichu et al., 2023; Knepp et al., 2024; Khaykin et al., 2022).

Overall, LOAC observations (Fig. 7) agree with POPS, with both instruments detecting exclusively particles $< 1\ \mu$m and a peak concentration below 100 nm. Particles $< 1\ \mu$m have also already been observed for the fresh plume within one week of the eruption by LOAC (Kloss et al., 2022). POPS shows systematically higher concentrations—by $\sim$20% to 90%—except in the 200–250 nm radius range. These differences fall mainly within the respective measurement uncertainties (c.f. Section 2.1 and 2.2).

Based on a lognormal fit, LOAC data yield an effective radius of 304 nm, consistent with POPS. A second mode seems possible in LOAC observations but shifted towards smaller particle sizes. However, unlike POPS, the bimodal distribution does not significantly improve the fit compared to a unimodal one. Because LOAC observations are limited to particles larger than the observed peak concentration (at around 100 nm) within the Hunga plume, lognormal fit analysis cannot work as reliably as for POPS. Therefore, parameters such as the effective radius (304 nm) and mode radius (41.7 nm), calculated with LOAC observations here, should be interpreted with caution.

3.5 The radiative impact of the Hunga eruption on the Northern Hemisphere

The observed perturbations to the northern-hemispheric stratospheric aerosol layer due to the transport of the Hunga plume have been used to quantify the inherent top-of-atmosphere (TOA) radiative forcing, using the UVSPEC radiative transfer model.
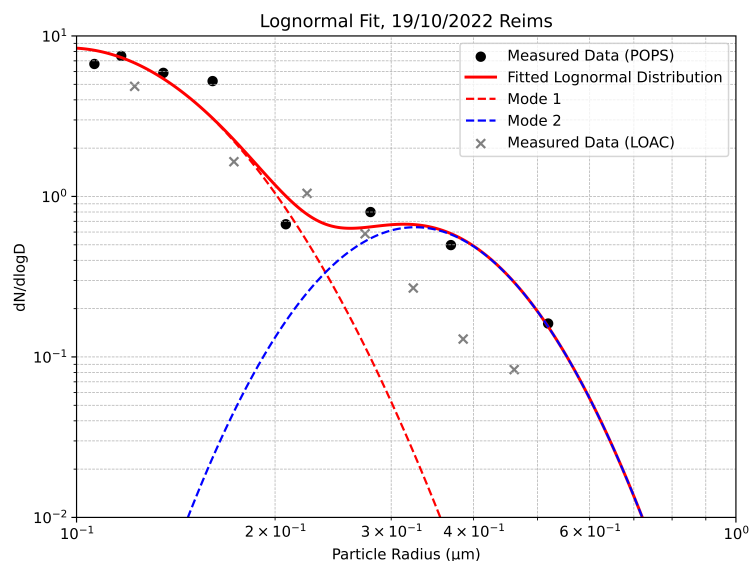
Figure 7. POPS and LOAC observations 19/10/2022 in Reims, France , as also presented in Fig. 1, for 20-22.5 km altitude. Black dots indicate POPS measurements, grey crosses represent the respective LOAC measurements. The red solid line represents the bimodal lognormal fit for POPS observations, the dashed lines represent the fits for the separate modes.

The strongest cumulative impact of the transported compact plume patches discussed above is observed from satellite between
265 November 2022 and April 2023 at altitudes of 16–24 km (see Fig. 1). Thus, we calculated the TOA radiative forcing using, as aerosol input, satellite aerosol extinction profiles observed during this period, with respect to a background for November 2017–April 2018 (the latest available period without major stratospheric perturbations, for this latitude region), latitudinally averaged between 30° and 50°N. As satellite inputs, we use those from SAGE III/ISS, which have a better signal-to-noise ratio than OMPS-LP and more reliable spectral information. Stratospheric aerosol extinction coefficient profiles for these two
270 periods, from SAGE III/ISS observations, are shown in Fig. 8.

The Hunga plume transported to the NH produced up to a 50% increase in the aerosol extinction coefficient, with respect to background conditions, on average, between about 16 and 24 km altitude. The visible-range AOD of the Hunga plume is found to be between about 2×10^{-3} and 1×10^{-3}, depending on the wavelength of the SAGE III/ISS observations, e.g., $(1.1 \pm 0.1) \times 10^{-3}$ at 756 nm (Table 2). This produced an increase in the Hunga-perturbed sAOD (to about 9×10^{-3} to 3×10^{-3},
275 depending on the wavelength, with $(4.1 \pm 0.5) \times 10^{-3}$ at 756 nm) with respect to the background stratosphere (at about 7×10^{-3} to 2×10^{-3}, depending on the wavelength, with $(3.1 \pm 0.5) \times 10^{-3}$ at 676 nm).

Using the different spectral AOD values obtained with SAGE III/ISS for the isolated Hunga plume in the NH, an Ångström exponent of (1.0 ± 0.2) is found (Table 2), which is very similar to both experimental values (Sellitto et al., 2024b) and theoretical values (Sellitto et al., 2024a) obtained for the main plume in the SH. Based on southern hemispheric aerosol optical
280 properties of the Hunga plume (single scattering albedo and phase function), estimated by Sellitto et al. (2024a) with a Mie
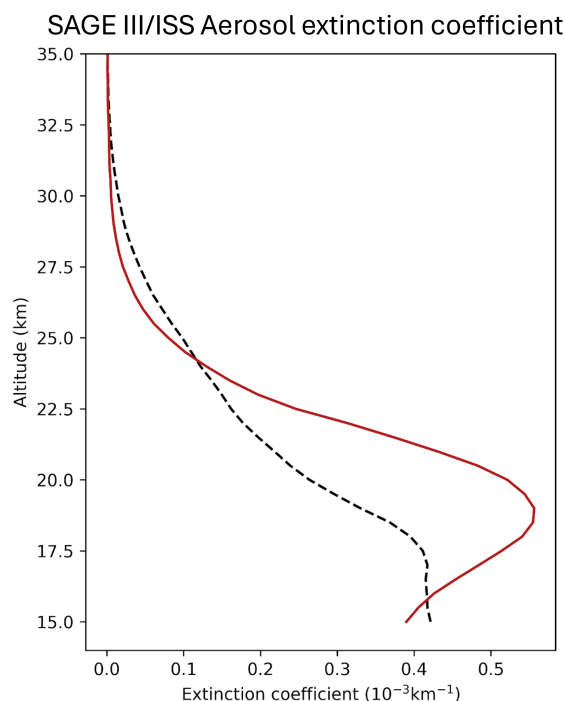
Figure 8. Average SAGE III/ISS stratospheric aerosol extinction coefficient profiles, between $30°$ and $50°$N, for a Hunga-perturbed period (November 2022–April 2023, solid red curve) and for a corresponding background period (November 2017–April 2018, dashed black curve), at 756 nm.

code, the assumption of pure sulphate aerosol particles, and size distributions obtained with satellite observations, a TOA radiative forcing of -0.05 ± 0.01 W m^{-2} is calculated (Table 2). This value, though small, is not negligible and is comparable to remote transport of other stratospheric aerosol plume patches (Kloss et al., 2019).

Please note that these shortwave estimations were obtained in the spectral interval covered by SAGE III/ISS (384 to 1550 nm), while the usual shortwave spectral range of integration should cover a larger range (e.g., 300–3000 nm, see Sellitto et al. (2022)); thus, the obtained values of the radiative forcing might be slightly underestimated.

4 Conclusions

While the Hunga eruption occurred in the SH, with its stratospheric and radiative impacts primarily confined to the SH and tropical regions, our findings show that parts of the aerosol plume were also transported into the NH stratosphere consistent with a direct transport pathway between the tropics and midlatitudes in the first few kilometers above the tropical tropopause, in which two-way mixing leads to tracer transport between the midlatitudes and the tropics. Dense plume segments were trans-

Table 2. Different optical and radiative properties of the Hunga plume transported to the NH are summarized as follows: average aerosol optical depth (AOD) at 676 nm is reported for the background stratosphere (October 2017–April 2018), the Hunga-perturbed stratosphere (October 2022–April 2023), and the isolated Hunga impact, calculated between 30° and 50°N. These values are derived from SAGE III/ISS extinction coefficients integrated between 15 km and the top of the atmosphere (TOA). The Ångström exponent is obtained by fitting the spectral SAGE III/ISS AOD observations using the Ångström power-law relation. The shortwave TOA radiative forcing is computed using the UVSPEC radiative transfer model.

Parameter	Value
$\langle AOD_{756\,nm}\rangle$ Oct 2017–Apr 2018	$(3.1 \pm 0.5) \times 10^{-3}$
$\langle AOD_{756\,nm}\rangle$ Oct 2022–Apr 2023	$(4.1 \pm 0.5) \times 10^{-3}$
$\langle AOD_{756\,nm}\rangle$ Hunga	$(1.1 \pm 0.1) \times 10^{-3}$
Ångström Exponent	1.0 ± 0.2
SW TOA RF	$-0.05 \pm 0.01 \ \mathrm{W\,m^{-2}}$

ported poleward, toward the northern mid-latitudes within this lower branch of the Brewer-Dobson Circulation.

Horizontal distribution analyses using OMPS-LP data reveal that aerosol transport into the NH began by February 2022 and persisted through mid-2023. By October, substantial aerosol enhancements extended up to 50°N, consistent with in situ mea-

295 surements. Aerosol transport occurred predominantly at altitudes of 17–23 km, with dense plumes observed at 21–22 km. During this period, the stratospheric aerosol extinction coefficient increased by approximately 50% compared to background conditions within the 30–50°N latitude band. This corresponds to an increase in AOD of approximately $(1-2) \times 10^{-3}$, depending on wavelength.

These aerosol enhancements resulted in a shortwave top-of-atmosphere (TOA) radiative forcing of $-0.05 \pm 0.01\,\mathrm{W\ m^{-2}}$, aver-

300 aged over 30–50°N from October 2022 to April 2023. While small, this forcing is not negligible and is comparable to radiative impacts observed from long-range transport of other stratospheric aerosol events.

These results underscore that even a volcanic eruption with moderate aerosol output can have measurable effects in the opposite hemisphere, with potentially significant consequences for regional radiative balance. Furthermore, the elevated aerosol load of the Hunga plume in the NH may enhance heterogeneous chemical reactions, with possible implications for ozone depletion and

305 polar stratospheric cloud formation. These effects should be taken into account in both global and regional chemistry-climate simulations.

Data availability. For the access of the OMPS v 2.0 data, they are available at

https://disc.gsfc.nasa.gov/datasets/OMPS_NPP_LP_L2_AER_DAILY_2/summary (NASA EarthData registration required). The SAGE III/ISS Aerosol Product can be accessed under

310 https://asdc.larc.nasa.gov/project/SAGEIII-ISS/g3bsspb_53. LOAC and POPS observations can be accessed via https://zenodo.org/records/15296481 and https://zenodo.org/records/15296481. POPC and COBALD data can be downloaded via figshare at https://doi.org/10.6084/m9.figshare.28887050.v1.
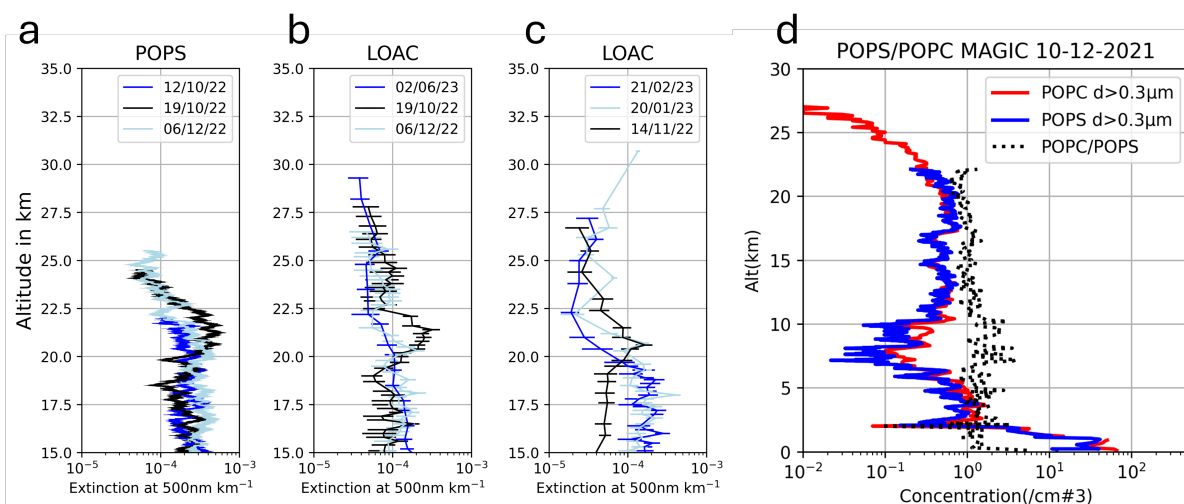
Figure A1. (a) to (c) Zoom plots respective to Figure 2 a-c. (d) Concentration observations for particles >0.3 um on 12/10/2022 in Reims, France for POPC (red) and POPS (blue). The relative difference is displayed with the dashed line.

Data for CALIPSO can be found at https://asdc.larc.nasa.gov/project/CALIPSO. The code for the CLaMS trajectory module is available on a GitLab server at https://jugit.fz-juelich.de/clams/CLaMS (Müller and the CLaMS team, 2024).

Video supplement. Complementary to Figure 6 and Section 3.3, the supplementary Video shows OMPS aerosol extinction observations at
315 21 to 22 km in the NH, from the beginning of 2021 to mid-2023 in 3-day-steps. The year 2021 is represented to represent aerosol extinction conditions before the Hunga eruption in January 2022, including the influence of the Soufrière eruption in 2021.

Appendix A

Comparison of the POPS observations from 12/10/2022, as shown in Figure 2, with coinciding POPC observations are shown in Figure A1d. A small balloon-borne Profiling Optical Particle Counter (OPC) (<2kg) was developed from the Particle Plus
320 8306 OPC (POPC) instrument for weather balloon applications. This POPC measures aerosol concentration profiles at eight radii between 0.15-5 μm from the ground to the stratosphere with 30 channels. The system employs a laser diode emitting at 785 nm. As particles enter the optical chamber, the scattered light at 90 degrees is amplified and converted into a voltage using a high-speed ADC (analog-to-digital converter), providing a digital measurement of the pulse height (Vernier et al., 2025, in preparation). In Fig. A1, both POPS and POPC aerosol concentration profiles show remarkable similar aerosol structures in
325 the stratosphere above 12 km with differences within 30%. At that time, there was no evidence for the transport of the Hunga plume in the NH.
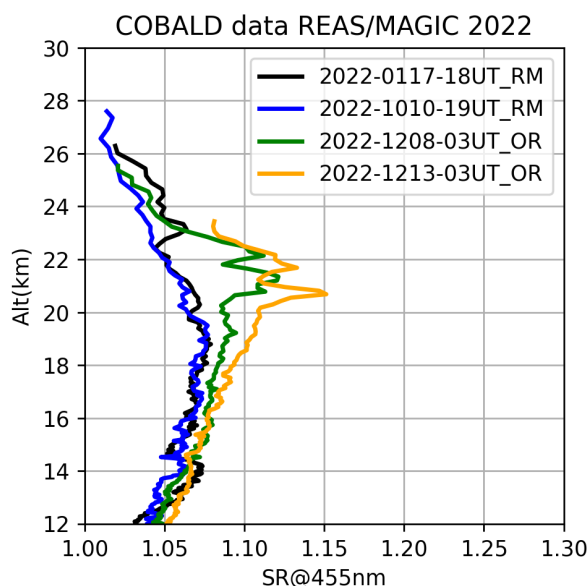
Figure A2. COBALD scatterin ratio observations at 455 nm from Reims, France in October and December 2022.

COBALD scattering ratio at 455 nm is shown for 4 flights from France in 2022 in Figure A2. COBALD is a lightweight (540 g) instrument that consists of two high-power light-emitting diodes (LEDs) that emit about 500 mW of optical power, at wavelengths of 455 and 940 nm, respectively. The backscattered light from the molecules, aerosols, or ice particles is recorded by a silicon photodiode using phase-sensitive detection. The precision along the backscatter ratio profile is better than 1% in the UTLS region (Brabec et al., 2012; Vernier et al., 2015). The first flight as shown in Fig. A2 took place on 17/01/2022 just after the Hunga eruption but before the plume could be transported in the NH. The transport of the Hunga is evident on 08/12 and 13/12 where scattering ratios are observed between 20 and 23 km with values reaching 1.15 in contrast with earlier measurements in October when the plume had not yet been transported over France as also suggested by Fig. 5. COBALD observations confirm a more significant aerosol signature in the NH mid-latitudes in December, compared to mid-October as also observed in Figure 1 and 4.

Author contributions. CK coordinated and designed the research. GB performed and coordinated in situ measurement campaigns and the respective funding. PS performed radiative offline simulations, respective analysis. RCD and JPV contributed CALIPSO Backscatter Initialized LaTM Trajectory Analysis. PM performed statistical fit analysis to in situ observations. JBR was responsible for LOAC data retrievals. IBG performed CLaMS trajectory simulations. GB, JBR, JPV, ND, LJ, SC, TL, GC and EB assisted in performing in situ observations. MIH, FP helped with transport analysis. All the authors contributed to the writing and revision of the paper.
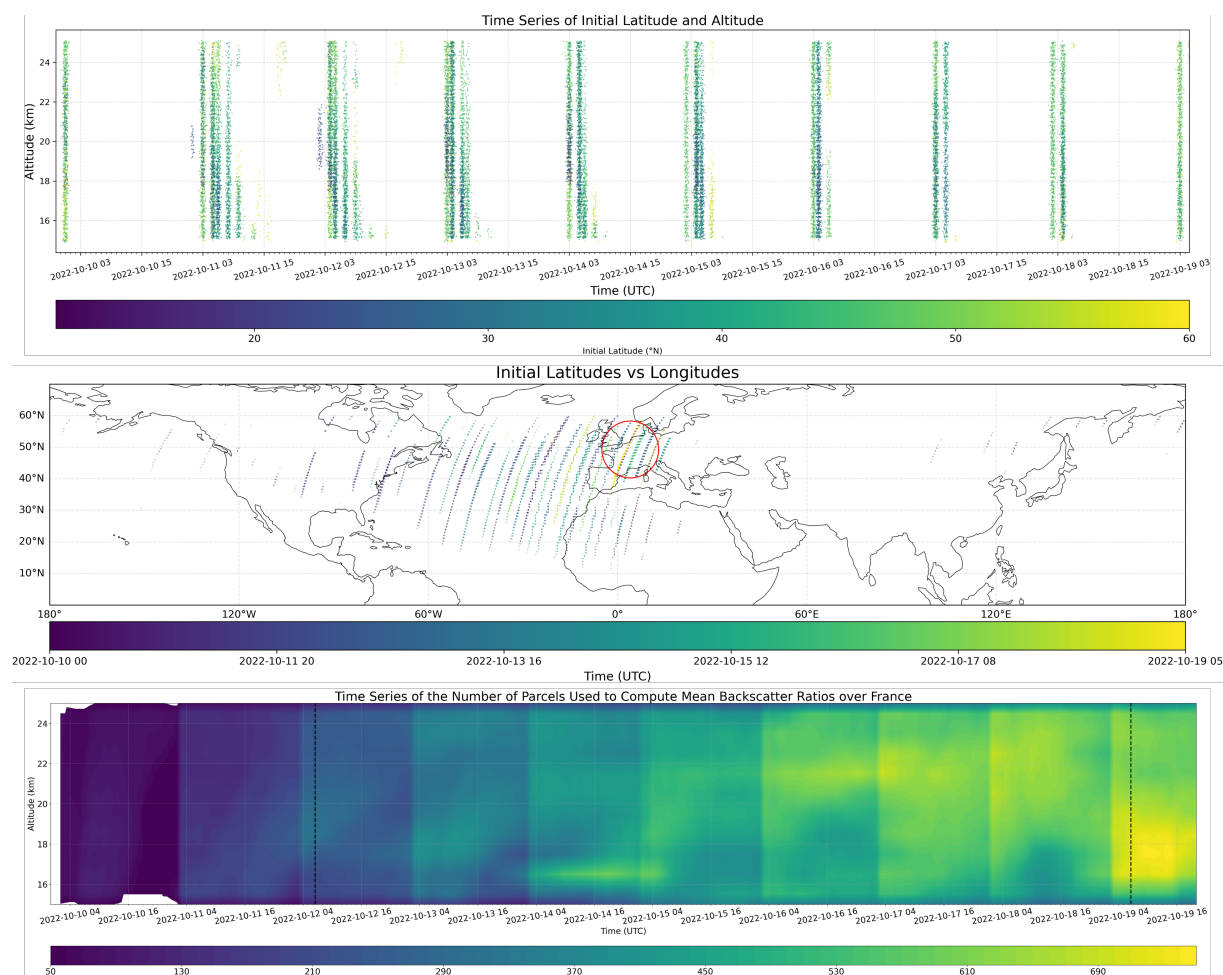
Figure A3. Time series of initial latitude and altitude (top), initial latitudes versus longitudes with the date of initializations depicted as a color bar (middle), and time series showing the number of parcels used to compute mean backscatter ratios over France (bottom).

Competing interests. The authors declare that they have no competing interests.

Acknowledgements. The authors are grateful to the National Aeronautics and Space Administration (NASA), SAGE III/ISS and OMPS teams. AI tools have been used to improve parts of the phrasing of the manuscript. We would like to thank Gilles Chalumeau and Thierry

345   Vincent for intensive technical work and help with the instrument and measurements. LPC2E gratefully acknowledges funding from the Labex Voltaire (ANR-10-LABX-100-01), the ASTuS ANR project (21-CE01-0007-01) and LE STUDIUM région Centre-Val de Loire for supporting JP Vernier's visit to LPC2E. This research has been partially supported by the Centre National d'Etudes Spatiales (grant no. EXTRA-SAT). We thank Gilles Chalumeau and Thierry Vincent for balloon flight preparation and operations in Orléans and the administrative team from National Institute of Aerospace, Amit Pandit and Johnny Mau for preparing payloads for the balloon flights conducted

350   in Reims, France. We thank the European Centre for Medium-Range Weather Forecasts (ECMWF) for providing the ERA5 reanalyses. The authors gratefully acknowledge the Gauss Centre for Supercomputing e.V. (www.gauss-centre.eu) for funding this project by providing computing time through the John von Neumann Institute for Computing (NIC) on the GCS Supercomputer JUWELS (Jülich Supercomputing Centre, 2021) at Jülich Supercomputing Centre (JSC). We thank the NASA Upper Atmospheric Composition Observation program and SAGE III/ISS science team for supporting the NIA/NASA teams.

References

Anderson, G., Clough, S., Kneizys, F., and Shettle, E.: AFGL Atmospheric Constituent Profiles (0.120km), AFGL Environmental Research Papers, pp. 1–46, https://apps.dtic.mil/dtic/tr/fulltext/u2/a175173.pdf, 1986.

Andersson, S. M., Martinsson, B. G., Vernier, J.-P., Friberg, J., Brenninkmeijer, C. A. M., Hermann, M., van Velthoven, P. F. J., and Zahn, A.: Significant radiative impact of volcanic aerosol in the lowermost stratosphere, Nature Communications, 6, 7692, https://doi.org/10.1038/ncomms8692, 2015.

Asher, E., Todt, M., Rosenlof, K., Thornberry, T., Gao, R.-S., Taha, G., Walter, P., Alvarez, S., Flynn, J., Davis, S. M., Evan, S., Brioude, J., Metzger, J.-M., Hurst, D. F., Hall, E., and Xiong, K.: Unexpectedly rapid aerosol formation in the Hunga Tonga plume, Proceedings of the National Academy of Sciences, 120, e2219547 120, https://doi.org/10.1073/pnas.2219547120, 2023.

Bian, J., Li, D., Bai, Z., Xu, J., Li, Q., Wang, H., Vömel, H., Wienhold, F. G., and Peter, T.: First detection of aerosols of the Hunga Tonga eruption in the Northern Hemisphere stratospheric westerlies, Science Bulletin, 68, 574–577, https://doi.org/https://doi.org/10.1016/j.scib.2023.03.002, 2023.

Boichu, M., Grandin, R., Blarel, L., Torres, B., Derimian, Y., Goloub, P., Brogniez, C., Chiapello, I., Dubovik, O., Mathurin, T., Pascal, N., Patou, M., and Riedi, J.: Growth and Global Persistence of Stratospheric Sulfate Aerosols From the 2022 Hunga Tonga–Hunga Ha'apai Volcanic Eruption, Journal of Geophysical Research: Atmospheres, 128, e2023JD039 010, https://doi.org/https://doi.org/10.1029/2023JD039010, e2023JD039010 2023JD039010, 2023.

Brabec, M., Wienhold, F. G., Luo, B. P., Vömel, H., Immler, F., Steiner, P., Hausammann, E., Weers, U., and Peter, T.: Particle backscatter and relative humidity measured across cirrus clouds and comparison with microphysical cirrus modelling, Atmospheric Chemistry and Physics, 12, 9135–9148, https://doi.org/10.5194/acp-12-9135-2012, 2012.

Brock, C. A., Froyd, K. D., Dollner, M., Williamson, C. J., Schill, G., Murphy, D. M., Wagner, N. J., Kupc, A., Jimenez, J. L., Campuzano-Jost, P., Nault, B. A., Schroder, J. C., Day, D. A., Price, D. J., Weinzierl, B., Schwarz, J. P., Katich, J. M., Wang, S., Zeng, L., Weber, R., Dibb, J., Scheuer, E., Diskin, G. S., DiGangi, J. P., Bui, T., Dean-Day, J. M., Thompson, C. R., Peischl, J., Ryerson, T. B., Bourgeois, I., Daube, B. C., Commane, R., and Wofsy, S. C.: Ambient aerosol properties in the remote atmosphere from global-scale in situ measurements, Atmospheric Chemistry and Physics, 21, 15 023–15 063, https://doi.org/10.5194/acp-21-15023-2021, 2021.

Bruckert, J., Hirsch, L., Horváth, Á., Kahn, R. A., Kölling, T., Muser, L. O., Timmreck, C., Vogel, H., Wallis, S., and Hoshyaripour, G. A.: Dispersion and Aging of Volcanic Aerosols After the La Soufrière Eruption in April 2021, Journal of Geophysical Research: Atmospheres, 128, e2022JD037 694, https://doi.org/https://doi.org/10.1029/2022JD037694, e2022JD037694 2022JD037694, 2023.

Carn, S. A., Krotkov, N. A., Fisher, B. L., and Li, C.: Out of the blue: Volcanic SO2 emissions during the 2021–2022 eruptions of Hunga Tonga—Hunga Ha'apai (Tonga), Frontiers in Earth Science, 10, https://doi.org/10.3389/feart.2022.976962, 2022.

Carr, J. L., Horváth, Á., Wu, D. L., and Friberg, M. D.: Stereo Plume Height and Motion Retrievals for the Record-Setting Hunga Tonga-Hunga Ha'apai Eruption of 15 January 2022, Geophysical Research Letters, 49, e2022GL098 131, https://doi.org/https://doi.org/10.1029/2022GL098131, e2022GL098131 2022GL098131, 2022.

Dahlback, A. and Stamnes, K.: A new spherical model for computing the radiation field available for photolysis and heating at twilight, Planetary and Space Science, 39, 671 – 683, https://doi.org/https://doi.org/10.1016/0032-0633(91)90061-E, 1991.

Deng, C., Li, Y., Yan, C., Wu, J., Cai, R., Wang, D., Liu, Y., Kangasluoma, J., Kerminen, V.-M., Kulmala, M., and Jiang, J.: Measurement report: Size distributions of urban aerosols down to 1 nm from long-term measurements, Atmospheric Chemistry and Physics, 22, 13 569–13 580, https://doi.org/10.5194/acp-22-13569-2022, 2022.

Deshler, T., Kalnajs, L. E., Norgren, M., Zhu, Y., and Zhang, J.: In Situ Aerosol Size Spectra Measurements in the Austral Polar Vortex Before and After the Hunga Tonga-Hunga Ha'apai Volcanic Eruption, Geophysical Research Letters, 51, e2024GL111388, https://doi.org/https://doi.org/10.1029/2024GL111388, e2024GL111388 2024GL111388, 2024.

395 Duchamp, C., Wrana, F., Legras, B., Sellitto, P., Belhadji, R., and von Savigny, C.: Observation of the Aerosol Plume From the 2022 Hunga Tonga—Hunga Ha'apai Eruption With SAGE III/ISS, Geophysical Research Letters, 50, e2023GL105076, https://doi.org/https://doi.org/10.1029/2023GL105076, e2023GL105076 2023GL105076, 2023.

Fairlie, T. D., Vernier, J.-P., Natarajan, M., and Bedka, K. M.: Dispersion of the Nabro volcanic plume and its relation to the Asian summer monsoon, Atmospheric Chemistry and Physics, 14, 7045–7057, https://doi.org/10.5194/acp-14-7045-2014, 2014.

400 Grant, W. B., Browell, E. V., Fishman, J., Brackett, V. G., Veiga, R. E., Nganga, D., Minga, A., Cros, B., Butler, C. F., Fenn, M. A., Long, C. S., and Stowe, L. L.: Aerosol-associated changes in tropical stratospheric ozone following the eruption of Mount Pinatubo, Journal of Geophysical Research: Atmospheres, 99, 8197–8211, https://doi.org/https://doi.org/10.1029/93JD03314, 1994.

Guo, S., Bluth, G. J. S., Rose, W. I., Watson, I. M., and Prata, A. J.: Re-evaluation of SO2 release of the 15 June 1991 Pinatubo eruption using ultraviolet and infrared satellite sensors, Geochemistry, Geophysics, Geosystems, 5, https://doi.org/https://doi.org/10.1029/2003GC000654, 2004.

405 Haynes, P. and Shuckburgh, E.: Effective diffusivity as a diagnostic of atmospheric transport: 1. Stratosphere, Journal of Geophysical Research: Atmospheres, 105, 22 777–22 794, https://doi.org/https://doi.org/10.1029/2000JD900093, 2000.

Hegglin, M. I. and Shepherd, T. G.: O3-N2O correlations from the Atmospheric Chemistry Experiment: Revisiting a diagnostic of transport and chemistry in the stratosphere, Journal of Geophysical Research: Atmospheres, 112, https://doi.org/https://doi.org/10.1029/2006JD008281, 2007.

410 Hersbach, H., Bell, B., Berrisford, P., Hirahara, S., Horányi, A., Muñoz-Sabater, J., Nicolas, J., Peubey, C., Radu, R., Schepers, D., Simmons, A., Soci, C., Abdalla, S., Abellan, X., Balsamo, G., Bechtold, P., Biavati, G., Bidlot, J., Bonavita, M., De Chiara, G., Dahlgren, P., Dee, D., Diamantakis, M., Dragani, R., Flemming, J., Forbes, R., Fuentes, M., Geer, A., Haimberger, L., Healy, S., Hogan, R. J., Hólm, E., Janisková, M., Keeley, S., Laloyaux, P., Lopez, P., Lupu, C., Radnoti, G., de Rosnay, P., Rozum, I., Vamborg, F., Villaume, S., and Thépaut, J.-N.: The ERA5 global reanalysis, Quarterly Journal of the Royal Meteorological Society, 146, 1999–2049, https://doi.org/https://doi.org/10.1002/qj.3803, 2020.

415 Homeyer, C. R. and Bowman, K. P.: Rossby Wave Breaking and Transport between the Tropics and Extratropics above the Subtropical Jet, Journal of the Atmospheric Sciences, 70, 607 – 626, https://doi.org/10.1175/JAS-D-12-0198.1, 2013.

Jaross, G., Bhartia, P. K., Chen, G., Kowitt, M., Haken, M., Chen, Z., Xu, P., Warner, J., and Kelly, T.: OMPS

420 Limb Profiler instrument performance assessment, Journal of Geophysical Research: Atmospheres, 119, 4399–4412, https://doi.org/https://doi.org/10.1002/2013JD020482, 2014.

Jülich Supercomputing Centre: JUWELS Cluster and Booster: Exascale Pathfinder with Modular Supercomputing Architecture at Juelich Supercomputing Centre, Journal of Large-Scale Research Facilities, 7, A183, https://doi.org/10.17815/jlsrf-7-183, 2021.

Khaykin, K., Podglajen, A., Ploeger, F., Grooß, J.-U., Tence, F., Bekki, S., Khlopenkov, K., Bedka, K., Rieger, L., Baron, A., Godin-

425 Beekmann, S., Legras, B., Sellitto, P., Sakai, T., Barnes, J., Uchino, O., Morino, I., Nagai, T., Wing, R., Baumgarten, G., Gerding, M., Duflot, V., Payen, G., Jumelet, J., and Ravetta, F.: Global perturbation of stratospheric water and aerosol burden by Hunga eruption, Communications Earth & Environment, 3, 316, https://doi.org/https://doi.org/10.1038/s43247-022-00652-x, 2022.

Kloss, C., Berthet, G., Sellitto, P., Ploeger, F., Bucci, S., Khaykin, S., Jégou, F., Taha, G., Thomason, L. W., Barret, B., Le Flochmoen, E., von Hobe, M., Bossolasco, A., Bègue, N., and Legras, B.: Transport of the 2017 Canadian wildfire plume to the tropics via the Asian

430   monsoon circulation, Atmospheric Chemistry and Physics, 19, 13 547–13 567, https://doi.org/10.5194/acp-19-13547-2019, 2019.

Kloss, C., Sellitto, P., Renard, J.-B., Baron, A., Bègue, N., Legras, B., Berthet, G., Briaud, E., Carboni, E., Duchamp, C., Duflot, V., Jacquet, P., Marquestaut, N., Metzger, J.-M., Payen, G., Ranaivombola, M., Roberts, T., Siddans, R., and Jégou, F.: Aerosol Characterization of the Stratospheric Plume From the Volcanic Eruption at Hunga Tonga 15 January 2022, Geophysical Research Letters, 49, e2022GL099 394, https://doi.org/https://doi.org/10.1029/2022GL099394, e2022GL099394 2022GL099394, 2022.

435   Knepp, T. N., Kovilakam, M., Thomason, L., and Miller, S. J.: Characterization of stratospheric particle size distribution uncertainties using SAGE II and SAGE III/ISS extinction spectra, Atmospheric Measurement Techniques, 17, 2025–2054, https://doi.org/10.5194/amt-17-2025-2024, 2024.

Kurucz, R.: The solar spectrum:, Atmos Chem Phys, 5, 1855–1877, https://doi.org/10.5194/acp-5-1855-2005, 2005.

Legras, B., Duchamp, C., Sellitto, P., Podglajen, A., Carboni, E., Siddans, R., Grooß, J.-U., Khaykin, S., and Ploeger, F.: The evolution

440   and dynamics of the Hunga Tonga–Hunga Ha'apai sulfate aerosol plume in the stratosphere, Atmospheric Chemistry and Physics, 22, 14 957–14 970, https://doi.org/10.5194/acp-22-14957-2022, 2022.

Li, Y., Pedersen, C., Dykema, J., Vernier, J.-P., Vattioni, S., Pandit, A. K., Stenke, A., Asher, E., Thornberry, T., Todt, M. A., Bui, T. P., Dean-Day, J., and Keutsch, F. N.: *In situ* measurements of perturbations to stratospheric aerosol and modeled ozone and radiative impacts following the 2021 La Soufrière eruption, EGUsphere, 2023, 1–22, https://doi.org/10.5194/egusphere-2023-1891, 2023.

445   Mayer, B. and Kylling, A.: Technical note: The libRadtran software package for radiative transfer calculations - description and examples of use, Atmos Chem Phys, 5, 1855–1877, https://doi.org/10.5194/acp-5-1855-2005, 2005.

McKenna, D. S., Grooß, J.-U., Günther, G., Konopka, P., Müller, R., Carver, G., and Sasano, Y.: A new Chemical Lagrangian Model of the Stratosphere (CLaMS) 2. Formulation of chemistry scheme and initialization, Journal of Geophysical Research: Atmospheres, 107, ACH 4–1–ACH 4–14, https://doi.org/https://doi.org/10.1029/2000JD000113, 2002a.

450   McKenna, D. S., Konopka, P., Grooß, J.-U., Günther, G., Müller, R., Spang, R., Offermann, D., and Orsolini, Y.: A new Chemical Lagrangian Model of the Stratosphere (CLaMS) 1. Formulation of advection and mixing, Journal of Geophysical Research: Atmospheres, 107, ACH 15–1–ACH 15–15, https://doi.org/https://doi.org/10.1029/2000JD000114, 2002b.

Millán, L., Santee, M. L., Lambert, A., Livesey, N. J., Werner, F., Schwartz, M. J., Pumphrey, H. C., Manney, G. L., Wang, Y., Su, H., Wu, L., Read, W. G., and Froidevaux, L.: The Hunga Tonga-Hunga Ha'apai Hydration of the Stratosphere, Geophysical Research Letters, 49,

455   e2022GL099 381, https://doi.org/https://doi.org/10.1029/2022GL099381, e2022GL099381 2022GL099381, 2022.

Müller, R. and the CLaMS team: Chemical Lagrangian Model of the Stratosphere (CLaMS) code repository, https://jugit.fz-juelich.de/clams/CLaMS, last access: 4 January 2024, 2024.

Pierluissi, J. H. and Peng, G. S.: New molecular transmission band models for LOWTRAN, Optical Engineering, 24, 1985.

Ploeger, F., Diallo, M., Charlesworth, E., Konopka, P., Legras, B., Laube, J. C., Grooß, J.-U., Günther, G., Engel, A., and Riese, M.: The

460   stratospheric Brewer–Dobson circulation inferred from age of air in the ERA5 reanalysis, Atmospheric Chemistry and Physics, 21, 8393–8412, https://doi.org/10.5194/acp-21-8393-2021, 2021.

Plumb, R. A.: Stratospheric Transport, Journal of the Meteorological Society of Japan. Ser. II, 80, 793–809, https://doi.org/10.2151/jmsj.80.793, 2002.

Pommrich, R., Müller, R., Grooß, J.-U., Konopka, P., Ploeger, F., Vogel, B., Tao, M., Hoppe, C. M., Günther, G., Spelten, N., Hoffmann,

465   L., Pumphrey, H.-C., Viciani, S., D'Amato, F., Volk, C. M., Hoor, P., Schlager, H., and Riese, M.: Tropical troposphere to stratosphere

transport of carbon monoxide and long-lived trace species in the Chemical Lagrangian Model of the Stratosphere (CLaMS), Geoscientific Model Development, 7, 2895–2916, https://doi.org/10.5194/gmd-7-2895-2014, 2014.

Proud, S. R., Prata, A. T., and Schmauß, S.: The January 2022 eruption of Hunga Tonga-Hunga Ha'apai volcano reached the mesosphere, Science, 378, 554–557, https://doi.org/10.1126/science.abo4076, 2022.

470 Renard, J.-B., Dulac, F., Berthet, G., Lurton, T., Vignelles, D., Jégou, F., Tonnelier, T., Jeannot, M., Couté, B., Akiki, R., Verdier, N., Mallet, M., Gensdarmes, F., Charpentier, P., Mesmin, S., Duverger, V., Dupont, J.-C., Elias, T., Crenn, V., Sciare, J., Zieger, P., Salter, M., Roberts, T., Giacomoni, J., Gobbi, M., Hamonou, E., Olafsson, H., Dagsson-Waldhauserova, P., Camy-Peyret, C., Mazel, C., Décamps, T., Piringer, M., Surcin, J., and Daugeron, D.: LOAC: a small aerosol optical counter/sizer for ground-based and balloon measurements of the size distribution and nature of atmospheric particles – Part 1: Principle of measurements and instrument evaluation, Atmospheric Measurement
475 Techniques, 9, 1721–1742, https://doi.org/10.5194/amt-9-1721-2016, 2016.

Ricchiazzi, P., Yang, S., Gautier, C., and Sowle, D.: SBDART: A Research and Teaching Software Tool for Plane-Parallel Radiative Transfer in the Earth's Atmosphere, Bull Amer Meteo Soc, 79, 2101–2114, https://doi.org/10.1175/1520-0477(1998)079<2101:SARATS>2.0.CO;2, 1998.

Rosenlof, K. H., Tuck, A. F., Kelly, K. K., Russell III, J. M., and McCormick, M. P.: Hemispheric asymmetries in water va-
480 por and inferences about transport in the lower stratosphere, Journal of Geophysical Research: Atmospheres, 102, 13 213–13 234, https://doi.org/https://doi.org/10.1029/97JD00873, 1997.

Schoeberl, M. R., Wang, Y., Ueyama, R., Taha, G., Jensen, E., and Yu, W.: Analysis and Impact of the Hunga Tonga-Hunga Ha'apai Strato-spheric Water Vapor Plume, Geophysical Research Letters, 49, e2022GL100 248, https://doi.org/https://doi.org/10.1029/2022GL100248, e2022GL100248 2022GL100248, 2022.

485 Schoeberl, M. R., Wang, Y., Taha, G., Zawada, D. J., Ueyama, R., and Dessler, A.: Evolution of the Climate Forcing During the Two Years After the Hunga Tonga-Hunga Ha'apai Eruption, Journal of Geophysical Research: Atmospheres, 129, e2024JD041 296, https://doi.org/https://doi.org/10.1029/2024JD041296, e2024JD041296 2024JD041296, 2024.

Sellitto, P., Podglajen, A., Belhadji, R., Boichu, M., Carboni, E., Cuesta, J., Duchamp, C., Kloss, C., Siddans, R., Bègue, N., Blarel, L., Jégou, F., Khaykin, S., Renard, J.-B., and Legras, B.: Significant radiative impact of volcanic aerosol in the lowermost stratosphere,
490 Communications Earth & Environment, 3, 288, https://doi.org/10.1038/s43247-022-00618-z, 2022.

Sellitto, P., Belhadji, R., Legras, B., Podglajen, A., and Duchamp, C.: The optical properties of stratospheric aerosol layer perturbation of the Hunga volcano eruption of January 15th, 2022, EGUsphere, 2024, 1–19, https://doi.org/10.5194/egusphere-2024-1433, 2024a.

Sellitto, P., Siddans, R., Belhadji, R., Carboni, E., Legras, B., Podglajen, A., Duchamp, C., and Kerridge, B.: Observing the SO2 and Sulfate Aerosol Plumes From the 2022 Hunga Eruption With the Infrared Atmospheric Sounding Interferometer (IASI), Geophysical Research
495 Letters, 51, e2023GL105 565, https://doi.org/https://doi.org/10.1029/2023GL105565, e2023GL105565 2023GL105565, 2024b.

Shepherd, T. G.: The middle atmosphere, Journal of Atmospheric and Solar-Terrestrial Physics, 62, 1587–1601, https://doi.org/https://doi.org/10.1016/S1364-6826(00)00114-0, 2000.

Shikwambana, L., Sivakumar, V., and Xongo, K.: Tracking the Transport of SO2 and Sulphate Aerosols from the Tonga Volcanic Eruption to South Africa, Atmosphere, 14, https://doi.org/10.3390/atmos14101556, 2023.

500 Sicard, M., Baron, A., Ranaivombola, M., Gantois, D., Millet, T., Sellitto, P., Bègue, N., Bencherif, H., Payen, G., Marquestaut, N., and Duflot, V.: Radiative impact of the Hunga stratospheric volcanic plume: role of aerosols and water vapor over Réunion Island (21° S, 55° E), Atmospheric Chemistry and Physics, 25, 367–381, https://doi.org/10.5194/acp-25-367-2025, 2025.

Taha, G., Loughman, R., Zhu, T., Thomason, L., Kar, J., Rieger, L., and Bourassa, A.: OMPS LP Version 2.0 multi-wavelength aerosol extinction coefficient retrieval algorithm, Atmospheric Measurement Techniques, 14, 1015–1036, https://doi.org/10.5194/amt-14-1015-2021, 2021.

Taha, G., Loughman, R., Colarco, P. R., Zhu, T., Thomason, L. W., and Jaross, G.: Tracking the 2022 Hunga Tonga-Hunga Ha'apai Aerosol Cloud in the Upper and Middle Stratosphere Using Space-Based Observations, Geophysical Research Letters, 49, e2022GL100 091, https://doi.org/https://doi.org/10.1029/2022GL100091, e2022GL100091 2022GL100091, 2022.

Taylor, I. A., Grainger, R. G., Prata, A. T., Proud, S. R., Mather, T. A., and Pyle, D. M.: A satellite chronology of plumes from the April 2021 eruption of La Soufrière, St Vincent, Atmospheric Chemistry and Physics, 23, 15 209–15 234, https://doi.org/10.5194/acp-23-15209-2023, 2023.

Todt, M. A., Asher, E., Hall, E., Cullis, P., Jordan, A., Xiong, K., Hurst, D. F., and Thornberry, T.: Baseline Balloon Stratospheric Aerosol Profiles (B2SAP)—Systematic Measurements of Aerosol Number Density and Size, Journal of Geophysical Research: Atmospheres, 128, e2022JD038 041, https://doi.org/https://doi.org/10.1029/2022JD038041, e2022JD038041 2022JD038041, 2023.

Trepte, C. R. and Hitchman, M. H.: Tropical stratospheric circulation deduced from satellite aerosol data, Nature, 355, 626–628, https://doi.org/10.1038/355626a0, 1992.

Vernier, H., Quintão, D., Biazon, B., Landulfo, E., Souza, G., Santos, V. A., Lopes, J. S. F., Mendes, C. P. A., Matta, A. S. J. D., Damaris, K. P., Grosslin, B., Jorge, P. M. P. M., Andrade, M. D. F., Rastogi, N., Raj, A., Liu, H., Kovilakam, M., Fadnavis, S., Wienhold, F. G., Colombier, M., Boone, D. C., Berthet, G., Dumelie, N., Joly, L., and Vernier, J.-P.: Balloon Observations Suggesting Sea Salt Injection into the Stratosphere from Hunga Tonga-Hunga Ha'apai, EGUsphere, 2025, 1–37, https://doi.org/10.5194/egusphere-2025-924, 2025.

Vernier, J. P., Pommereau, J. P., Garnier, A., Pelon, J., Larsen, N., Nielsen, J., Christensen, T., Cairo, F., Thomason, L. W., Leblanc, T., and McDermid, I. S.: Tropical stratospheric aerosol layer from CALIPSO lidar observations, Journal of Geophysical Research: Atmospheres, 114, https://doi.org/https://doi.org/10.1029/2009JD011946, 2009.

Vernier, J.-P., Fairlie, T. D., Natarajan, M., Wienhold, F. G., Bian, J., Martinsson, B. G., Crumeyrolle, S., Thomason, L. W., and Bedka, K. M.: Increase in upper tropospheric and lower stratospheric aerosol levels and its potential connection with Asian pollution, Journal of Geophysical Research: Atmospheres, 120, 1608–1619, https://doi.org/https://doi.org/10.1002/2014JD022372, 2015.

Zhu, Y., Bardeen, C. G., Tilmes, S., Mills, M. J., Wang, X., Harvey, V. L., Taha, G., Kinnison, D., Portmann, R. W., Yu, P., Rosenlof, K. H., Avery, M., Kloss, C., Li, C., Glanville, A. S., Millán, L., Deshler, T., Krotkov, N., and Toon, O. B.: Perturbations in stratospheric aerosol evolution due to the water-rich plume of the 2022 Hunga-Tonga eruption, Communications Earth & Environment, 3, 248, https://doi.org/https://doi.org/10.1038/s43247-022-00580-w, 2022.